Inorganic Chemistry
Article

Inorg. Chem. **2010**, *49*, 10183–10190 **10183**
DOI: 10.1021/ic101471u

Persistent Metal Bis(Hexafluoroacetylacetonato) Complexes Featuring a 2,2′-Bipyridine Substituted Triarylamminium Radical Cation

Sharew Adugna,[†] Kseniya Revunova,[†] Brandon Djukic,[†] Serge I. Gorelsky,[‡] Hilary A. Jenkins,[§] and Martin T. Lemaire*[,†]

[†]*Department of Chemistry, Brock University, St.Catharines, Ontario L2S 3A1,* [‡]*Center for Catalysis Research and Innovation, Department of Chemistry, University of Ottawa, Ottawa, Ontario K1N 6N5, and* [§]*Department of Chemistry, McMaster University, Hamilton, Ontario L8S 4M1*

Received July 22, 2010

Herein, we describe the preparation of a 2,2′-bipyridine derivative containing a redox-active *N,N*′-(4,4′-dimethoxydiphenylamino) substituent (**1**), which readily coordinates M(hfac)$_2$ salts [M = Mn (**2**), Ni (**3**), Cu (**4**)] to generate stable, neutral, and pseudo-octahedral coordination complexes, which have been fully characterized. Cyclic voltammetry and spectroelectrochemical measurements on complexes **2**−**4** indicate stable one-electron oxidation processes, and the formation of persistent radical cation complexes. The neutral complexes (M = Mn or Ni) were subject to one-electron oxidation with $NOPF_6$ in acetonitrile, and magnetic moments of the resulting solutions were obtained using the Evans method at different temperatures. Our experimental results suggest that the first reported ferromagnetically coupled metal−triarylamminum radical cation complex is obtained when M = Mn^{2+}, and antiferromagnetic coupling results when M = Ni^{2+}. These results are supported by results from density functional theory calculations, which indicate that a π spin polarization mechanism for magnetic exchange coupling is operative in singly oxidized complexes, **2**−**4**.

Introduction

The *metal−radical approach* is a very well-established protocol geared toward the preparation of magnetic materials featuring strong exchange coupling.[1] The advantage provided by radical ligands is the generation of typically stronger intramolecular magnetic exchange coupling than is obtained via other superexchange mechanisms, whereby magnetic coupling between metal ions is mediated by diamagnetic bridging ligands. A large number of metal complexes have been reported with a variety of coordinated stable radicals, including nitroxides, verdazyls, thiazyls, and thioaminyls as well as other charged radical species like semiquinones, iminosemiquinones, and TCNE derivatives.[2−8] The majority of reported metal−radical complexes are monometallic, partly owing to the difficulty in stable radical ligand synthesis and stability of the resulting complexes. As a result, what remains virtually unexplored is the use of radical ligands to create polynuclear complexes exhibiting strong intracluster exchange coupling, which seems like a promising route toward high-spin complexes featuring ground spin states that are well isolated in energy from other higher lying spin excited states.[9] From a synthetic perspective, some of the known families of stable radicals are not easily amenable to the construction of larger polytopic architectures that would be required in this regard. However, there has been some progress in the creation of high-spin molecules using radical ligands as linkers, with, for example, charged radical species, such as semiquinones, and Shultz et al. have reported a number of interesting polynuclear complexes of tris(semiquinonyl) ligands.[10] In this manner, we are interested in the exploration of the coordination chemistry of substituted triarylamminium radical cations. Studies focused on the preparation and electronic properties of these nitrogen-centered radicals have been reported by Blackstock and coworkers, Lahti and co-workers, and others, including a number of recent reports which featured the isolation of high-spin polytriarylamminium radicals and other uses for triarylamminum

*To whom correspondence should be addressed. E-mail: mlemaire@brocku.ca.

(1) (a) Caneschi, A.; Gatteschi, D.; Sessoli, R.; Rey, P. *Acc. Chem. Res.* **1989**, *22*, 392–398. (b) Lemaire, M. T. *Pure Appl. Chem.* **2004**, *76*, 277–293.
(2) (a) Luneau, D.; Rey, P. *Coord. Chem. Rev.* **2005**, *249*, 2591–2611. (b) Caneschi, A; Gatteschi, D; Rey, P. *Prog. Inorg. Chem.* **1991**, *39*, 331–429. (c) Kaizaki, S. *Coord. Chem. Rev.* **2006**, *250*, 1804–1818.
(3) Koivisto, B. D.; Hicks, R. G. *Coord. Chem. Rev.* **2005**, *249*, 2612–2630.
(4) Preuss, K. E. *Dalton Trans.* **2007**, *23*, 2357–2369.
(5) Miura, Y.; Kato, I.; Teki, Y. *Dalton Trans.* **2006**, *7*, 961–966.
(6) Shultz, D. A. *Comment Inorg. Chem.* **2002**, *23*, 1–21.
(7) (a) Mukherjee, S.; Rentschler, E.; Weyhermueller, T.; Wieghardt, K.; Chaudhuri, P. *Chem. Commun.* **2003**, *15*, 1828–1829. (b) Dei, A.; Gatteschi, D.; Sangregorio, C.; Sorace, L.; Vaz, M. G. F. *Inorg. Chem.* **2003**, *42*, 1701–1706.
(8) (a) Miller, J. S. *Dalton Trans.* **2006**, *23*, 2742–2749. (b) Miller, J. S.; Epstein, A. J. *Chem. Commun.* **1998**, *13*, 1319–1325.
(9) (a) Vostrikova, K. E.; Luneau, D.; Wernsdorfer, W.; Rey, P.; Verdaguer, M. *J. Am. Chem. Soc.* **2000**, *122*, 718–719. (b) Caneschi, A.; Gatteschi, D.; Laugier, J.; Rey, P.; Sessoli, R.; Zanchini, C. *J. Am. Chem. Soc.* **1988**, *110*, 2795–2799.
(10) Caneschi, A.; Dei, A.; Mussari, C. P.; Shultz, D. A.; Sorace, L.; Vostrikova, K. E. *Inorg. Chem.* **2002**, *41*, 1086–1092.

Published on Web 10/05/2010

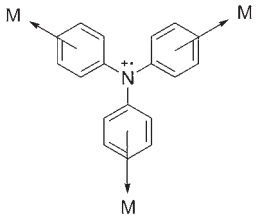

Figure 1. Substituted triarylamminium radical cation as a SCU toward high-spin polynuclear complexes.

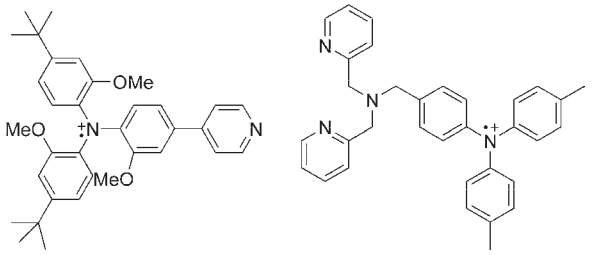

Figure 2. Left: 4-pyridyl-substituted triarylamminium radical cation (L) used to prepare $M(hfac)_2L_2$ complexes ($M = Mn^{2+}$ and Cu^{2+}). Right: 4-*bis*(2-picolyl)aminomethyl-substituted triarylamminium radical cation used to prepare a Cu^{2+} complex.

radicals in materials science.[11,12] Our approach is to use these radical cations as "spin coupling units" (SCU) and create high-spin polynuclear complexes making use of established π-topology spin coupling rules in our design (Figure 1).[13]

However, the coordination chemistry of triarylamminium radicals is nearly unexplored territory; reported complexes featuring triarylamminium radical cations are few and, to our knowledge, include only two published accounts. Bushby et al. reported the generation of persistent $M(hfac)_2$ (M = Mn, Cu) complexes containing monodentate 4-pyridyl-substituted triarylamminium radical cations as models to explore the utility of similar radicals toward 1-D coordination polymers (Figure 2).[14] In all cases, weak antiferromagnetic metal−radical exchange coupling was observed, owing in part to the large distance separating the triarylamminium spin from the metal center. The only other report was from Yano and included a Cu^{2+} complex containing a 4-bis(2-picolyl)aminomethyl-substituted triarylamminium radical in which EPR measurements indicated a very weak Cu^{2+}-radical magnetic interaction of an unknown nature (Figure 2).[15]

Our group is interested in the exploration of the coordination chemistry of substituted triarylamminium radical cations as a new class of redox-active ligands (RAL). Specifically, we are investigating complexes in which the triarylamminium spin is close to the metal center in an effort to enhance the metal−radical magnetic coupling. In this report, we describe the synthesis and characterization of **1** and a series of neutral $M(hfac)_2$ complexes (M^{2+} = Mn, Ni, Cu) containing **1**, including the electrochemical or chemical oxidation of these complexes to afford triarylamminium radical cation complexes. The radical cation complexes are characterized in part using spectroelectrochemical methods, and the magnetic properties of these complexes (M^{2+} = Mn, Ni) are investigated in solution using the Evans method. We propose a π spin polarization mechanism to describe the observed intramolecular metal−radical magnetic exchange coupling, which is corroborated by density functional theory (DFT) calculations of the spin distributions in each of the radical cation complexes.

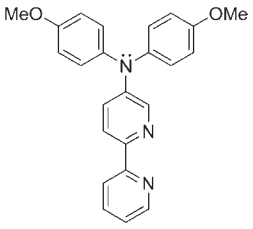

1

Experimental Section

General Procedures. All reagents were commercially available and used as received unless otherwise stated. Deaerated and anhydrous solvents were obtained from a Puresolve PS MD-4 solvent purification system, and all air- and/or moisture-sensitive reactions were carried out using standard Schlenk techniques. $^1H/^{13}C$ NMR spectra were recorded on a Bruker Advance 300 MHz spectrometer with a 7.05 T Ultrashield magnet using deuterated solvents. FT-IR spectra were recorded on a Shimadzu IRAffinity spectrometer as thin films deposited by evaporation of CH_2Cl_2 solutions on KBr plates. EI/FAB mass spectra were obtained using a Kratos Concept 1S High Resolution E/B mass spectrometer. UV−vis measurements were recorded on a Shimadzu 3600 UV−vis−NIR spectrophotometer in CH_2Cl_2 solution using quartz cuvette cells. Elemental analyses were carried out by Canadian Microanalytical Services, LTD, Surrey, British Columbia, Canada, or Guelph Chemical Laboratories LTD, Guelph, Ontario, Canada.

Electrochemical Measurements. Cyclic voltammetry (CV) experiments were performed with a Bioanalytical Systems, Inc. Epsilon electrochemical workstation. Compounds **1**−**4** were dissolved in anhydrous solvent (CH_3CN), filtered, and then deareated by sparging with N_2 gas for 20 min. Analyte concentrations were approximately 10^{-3} M containing 0.1 M supporting electrolyte (Bu_4NPF_6). A typical three-electrode setup was used, including a glassy carbon working electrode, Ag/AgCl reference electrode, and a platinum wire counter electrode. Ferrocene was used in all cases as an internal standard to calibrate the reference electrode and was oxidized at a potential of +0.51 V in our setup. The scan rate for all CV experiments was 100 mV/s or as otherwise stated in the text.

Spectroelectrochemical Measurements. Spectroelectrochemical experiments were performed in CH_2Cl_2 solution (10^{-5} M in 2−4) containing approximately 0.1 M supporting electrolyte (Bu_4NPF_6) using a Bioanalytical Systems, Inc. Epsilon electrochemical workstation. A special thin layer quartz glass cuvette containing the above solution in addition to a small platinum gauze working electrode, platinum wire counter electrode, and silver wire reference electrode was loaded into a Shimadzu UV-3600, and a constant potential of 1.0 V (versus ferrocene) was applied. UV−visible spectra were recorded in repeat mode (250−1000 nm),

(11) (a) Blackstock, S. C.; Selby, T. D. *Magnetic Properties of Organic Materials*; Lahti, P. M., Eds.; Marcel Dekker, Inc.: New York, 1999; pp 165−178. (b) Murata, H.; Lahti, P. M. *J. Org. Chem.* **2007**, *72*, 4974–4977.
(12) (a) Sakurai, H.; Izuoka, A.; Sugawara, T. *J. Am. Chem. Soc.* **2000**, *122*, 9723–9734. (b) Murata, H.; Takahashi, M.; Namba, K.; Takahashi, N.; Nishide, H. *J. Org. Chem.* **2004**, *69*, 631–638. (c) Fukuzaki, E.; Nishide, H. *J. Am. Chem. Soc.* **2006**, *128*, 996–1001. (d) Kurata, T.; Koshika, K.; Kato, F.; Kido, J.; Nishide, H. *Polyhedron* **2007**, *26*, 1776–1780. (e) Kurata, T.; Koshika, K.; Kato, F.; Kido, J.; Nishide, H. *Chem. Commun.* **2007**, 2986–2988.
(13) (a) Rajca, A. *Chem. Rev.* **1994**, *94*, 871–893. (b) Iwamura, H.; Koga, N. *Acc. Chem. Res.* **1993**, *26*, 346–351. (c) Iwamura, H. *Adv. Phys. Org. Chem.* **1990**, *26*, 179–253.
(14) Bushby, R. J.; Kilner, C.; Taylor, N.; Williams, R. A. *Polyhedron* **2008**, *27*, 383–392.
(15) Yano, M.; Inoue, K.; Motoyama, T.; Azuma, Y.; Tatsumi, M.; Yamauchi, O.; Oyama, M.; Sato, K.; Takui, T. *Polyhedron* **2005**, *24*, 2112–2115.
(16) (a) Sur, S. K. *J. Magn. Reson.* **1989**, *82*, 169–173. (b) Evans, D. F. *J. Chem. Soc.* **1959**, 2003–2005. (c) Chambers, J.; Eaves, B.; Parker, D.; Claxton, R.; Ray, P. S.; Slattery, S. J. *Inorg. Chim. Acta* **2006**, *359*, 2400–2406.

Table 1. Crystallographic Data for **4**

formula	$C_{34}H_{23}CuF_{12}N_3O_6$
fw	861.09
dimensions (mm)	0.266 × 0.135 × 0.095
a (Å)	10.2632(16)
b (Å)	30.851(5)
c (Å)	11.4269(18)
cryst syst	monoclinic
α (deg)	90
β (deg)	104.555(3)
γ (deg)	90
volume (Å^3)	3502.0(10)
space group	*Pc*
Z	4
μ (mm^{-1})	0.738
T (K)	100(2)
independent reflns	10 497 (R_{int} = 0.0830)
number of params	964
R_1 [$F^2 > 2\sigma(F^2)$]	0.0848
wR_2 (F^2)[a]	0.2239

[a] $w = 1/[\sigma^2(F_o^2) + (0.069P)^2 + 0.2902P]$ where $P = (F_o^2 + 2F_c^2)/3$.

until subsequent runs no longer resulted in any significant spectral changes.

X-Ray Structure Determination. Crystals of suitable size were mounted on a glass fiber. Data were collected at room temperature (100 K) on a SMART APEX II diffractometer with Mo Kα radiation (λ = 0.71073 Å) located at the McMaster Analytical X-ray Diffraction Facility (MAX); see Table 1 for crystallographic data for **4**. Data were processed using APEX v2.2.0 and solved by direct methods (SHELXS-97). Data were refined using least-squares techniques on F^2. The data were solved in the monoclinic space group *P*2 and checked by Platon AddSymm for additional symmetry. All non-hydrogen atoms were refined anisotropically except for those that were disordered (see below). Hydrogen atoms were generated and treated as riding on their constituent atoms with updates after each cycle of refinement. A 2-fold twin law was applied, with a resultant BASF of 0.13(2). The disordered groups for molecule 1 (Cu1) include CF3 (F1, F2, and F3), rotationally disordered over two positions in a 75:25 ratio, and the F atoms were restrained with EADP. The other disordered portion of molecule 1 is the anisole ring starting with C18, with a ring shift and methyl ether disorder of 80:20. These atoms were also restrained with EADP and refined isotropically. Similarly, for molecule 2, there are two CF3 groups with rotational disorder: F13, F14, and F15 at a ratio of 56:44 and F22, F23, and F24, at a 41:59 ratio. One of the anisole rings in this molecule was also disordered similar to that in molecule 1, at 45:55. All disordered atoms in molecule 2 were also refined isotropically. In the final stages of refinement, two peaks of residual electron density were located. The first was associated with O4 of the nondisordered ring of molecule 1, and the second with C113 of the nondisordered anisole of molecule 2. Attempts to refine these as atoms did not result in reasonable results, and it is assumed that these peaks are possibly "shadows" from the heavy atoms in a second crystal.

Variable-Temperature Magnetic Susceptibility Measurements and EPR Spectroscopy. Solid state variable-temperature magnetic susceptibility measurements were recorded on a superconducting quantum interference device (SQUID) magnetometer (Quantum Design MPMS) with a 5.5 T magnet (temperature range 1.8−400 K) in an external field of 0.5 T. Samples of **2**−**4** were carefully weighed into gelatin capsules, which were loaded into plastic straws, and attached to the sample transport rod. The magnetization of the samples was scanned over a temperature range of 5 to 325 K and then back to 5 K (for **3** and **4**), or from 5 to 325 K for **2**. Diamagnetic corrections to the paramagnetic susceptibilities were accomplished using Pascal's constants. Solution magnetic moments were obtained using the Evans method.[15] In a typical experiment, 29.1 mg of complex **2** was dissolved in exactly 4.0 mL of dry acetonitrile. Under N_2, one equivalent of $NOPF_6$ dissolved in exactly 1.0 mL of acetonitrile was added, resulting in a color change to dark green. The solution was stirred for approximately 10 min, and then a small portion was withdrawn by syringe under N_2 and loaded into a special narrow coaxial NMR tube assembly. This narrow tube was inserted into another NMR tube containing an approximately 1:1 mixture of CH_3CN and CD_3CN, and ^{1}H NMR spectra were immediately recorded at a series of different temperatures. Mass susceptibility (χ_g) was calculated from eq 1:

$$\chi_g = \frac{3\Delta\nu}{4\pi\nu c} \quad (1)$$

where $\Delta\nu$ is the difference in absorption frequency between CH_3CN in the outer and inner tubes, ν is the spectrometer frequency (600.32 MHz), and c is the concentration (g/mL) of the paramagnetic complex. Molar susceptibility was calculated in the typical manner, and corrections for the diamagnetism of the complex and solvent were calculated using Pascal's constants.[17] The temperature-dependent density changes of the acetonitrile solvent were accounted for using published values, and the required corrections were made to the paramagnetic solution concentrations. EPR spectra were recorded as toluene solutions at room temperature in quartz tubes on a BrukerElexsys E580 pulsed and CW X-band (9 GHz) spectrometer.

Computational Details

All DFT calculations were performed using the Gaussian 03 package using the B3LYP hybrid functional and the TZVP basis set for all atoms.[18] Tight SCF convergence criteria were used for all calculations. The converged wave functions were tested to confirm that they correspond to the ground-state surface. The evaluation of atomic charges and spin densities was performed using the natural population analysis (NPA).[19] The analysis of molecular orbitals in terms of fragment orbital contributions were carried out using the AOMix program.[20] Time-dependent DFT (TD-DFT) calculations at the B3LYP/TZVP level were performed to calculate the absorption spectra as previously described.[21]

Synthesis

Preparation of 5-(4,4′-dimethoxydiphenylamino)-2,2′-bipyridine (1). 5-Bromo-2,2′-bipyridine[22] (0.104 g, 0.442 mmol), *N*,*N*′-(4,4′-dimethoxydiphenyl)amine (0.125 g, 0.546 mmol), Cs_2CO_3 (0.202 g, 0.620 mmol), palladium-(II) acetate (0.0055 g, 0.0245 mmol), and BINAP (0.015 g, 0.024 mmol) were combined under N_2 into a dry Schlenk flask and slurried into dry toluene (20 mL). The solution was purged with N_2 for 20 min and then heated to 95 °C. Total consumption of starting materials was noted after 35 h, at which time the reaction was cooled to room temperature. The cooled reaction contents were filtered, and the precipitate was washed with $CHCl_3$. The filtrate and washing were rotovaped down to a brown oil, which

(17) Hatfield, W. E. *Theory and Application of Molecular Paramagnetism*; Boudreaux, E. A., Mulay, L. N., Eds.; Wiley and Sons: New York, 1976; pp 491−495.
(18) Schafer, A.; Huber, C.; Ahlrichs, R. *J. Chem. Phys.* **1994**, *100*, 5829–5835.
(19) (a) Godbout, N.; Salahub, D. R.; Andzelm, J.; Wimmer, E. *Can. J. Chem.* **1992**, *70*, 560–571. (b) Reed, A. E.; Curtiss, L. A.; Weinhold, F. *Chem. Rev.* **1988**, *88*, 899–926.
(20) Gorelsky, S. I. *AOMix*, version 6.46; University of Ottawa: Ottawa, Canada, 2010.
(21) Gorelsky, S. I.; Lever, A. B. P. *J. Organomet. Chem.* **2001**, *635*, 187–196.
(22) Fang, Y.-Q.; Hanan, G. S. *Synlett* **2003**, *6*, 852–854.

was chromatographed over neutral Al_2O_3 (12″ × 1″), eluting with 9:1 hex/EtOAc, followed by 7:3 hex/EtOAc (R_f = 0.6) to collect the bright yellow zone. Pure fractions were combined and concentrated to a white solid, yield: 130 mg (77%). ^{1}H NMR ($CDCl_3$): δ 8.63 (d, 1H, J = 4 Hz), 8.31 (d, 1H, J = 3 Hz), 8.28 (d, 1H, J = 8 Hz), 8.19 (d, 1H, J = 9 Hz), 7.76 (dd, 1H, J = 8, 2 Hz), 7.32 (dd, 1H, J = 9, 3 Hz), 7.23 (dd, 1H, J = 8, 2 Hz), 7.12 (d, 4H, J = 9 Hz), 6.89 (d, 4H, J = 9 Hz), 3.83 ppm (s, 6H). ^{13}C NMR ($CDCl_3$): δ 156.6, 156.0, 149.0, 147.4, 145.2, 140.9, 139.6, 136.7, 126.8, 126.3, 122.5, 121.0, 120.1, 115.0, 55.5 ppm. Anal. Calcd for $C_{24}H_{21}N_3O_2$ (Found): C, 75.16 (74.82); H, 5.52 (5.61); N, 10.96% (10.89%). MS (EI +): m/z 383 (M^+, 100%), 368 (M − CH_3, 30%). FT-IR (film, KBr): 3045 (w), 3001 (w), 2930 (w), 2833 (w), 1568 (m), 1541 (s), 1458 (s), 1435 (w), 1327 (m), 1242 (s), 1165 (w), 1033 (m), 827 (m), 739 (m), 638 (w), 581 cm^{-1} (w). UV−vis (CH_2Cl_2), λ_{max} (ε): 352 nm (2.1 × 10^4 cm^{-1} M^{-1}).

Mn(hfac)$_2$(1) (2). Mn(hfac)$_2\cdot$3H$_2$O (0.22 g, 0.42 mmol) was dissolved in a solvent mixture containing hexanes (5 mL) and MeOH (2 mL) and combined with a CH_2Cl_2 solution (5 mL) of **1** (0.15 g, 0.39 mmol). The solution was stirred at room temperature for 1 h to produce a clear, orange solution. The solution was filtered and left standing at room temperature. Over a period of days, orange, rod-shaped crystals were observed, which were isolated by vacuum filtration, yield: 0.14 g, (41%). Anal. Calcd for $C_{34}H_{23}N_3O_6F_{12}Mn$ (Found): C, 47.88 (48.05); H, 2.72 (2.43); N, 4.93 (4.98). MS (FAB +): 852 (M^+, 2), 645 (M − hfac, 50), 383 (**1**, 100%). FT-IR (film, KBr): 1651 (m), 1589 (w), 1557 (m), 1508 (s), 1470 (s), 1442 (m), 1344 (m), 1252 (s), 1196 (s), 1142 (s), 1082 (w), 1032 (w), 833 (w), 795 (m), 662 (m), 583 cm^{-1} (w). UV−vis (CH_2Cl_2), λ_{max} (ε): 385 nm (1.8 × 10^4 cm^{-1} M^{-1}).

Ni(hfac)$_2$(1) (3). Ni(hfac)$_2\cdot$2H$_2$O (0.13 g, 0.26 mmol) was slurried in 7 mL of hexanes and combined with a CH_2Cl_2 solution (4 mL) of **1** (0.10 g, 0.26 mmol). The solution was stirred at room temperature overnight to produce a clear, golden solution. The solution was concentrated to a crusty golden residue, which was dissolved into hot hexanes (12 mL). Upon cooling to room temperature, a green microcrystalline powder precipitated, which was isolated by vacuum filtration, yield: 0.14 g (61%). Anal. Calcd for $C_{34}H_{23}N_3O_6F_{12}Ni$ (Found): C, 47.67 (47.86); H, 2.71 (2.78); N: 4.91 (4.95). MS (EI +): 648 (M-hfac, 10%), 383 (**1**, 100%). FT-IR (film, KBr): 1643 (m), 1590(w), 1556 (m), 1506 (s), 1471 (s), 1441 (m), 1346 (m), 1256 (s), 1202 (s), 1148 (s), 1097 (m), 1034 (m), 833 (w), 791 (m), 671 (m), 586 cm^{-1} (m). UV−vis (CH_2Cl_2), λ_{max} (ε): 383 nm (1.8 × 10^4 cm^{-1} M^{-1}).

Cu(hfac)$_2$(1) (4). Cu(hfac)$_2\cdot x$H$_2$O (0.068 g, 0.14 mmol) was slurried in 7 mL of 2:1 hexanes/CH_2Cl_2 and combined with a CH_2Cl_2 solution (2 mL) of **1** (0.055 g, 0.14 mmol). The solution was stirred at room temperature for 3 h to produce a clear red-brown solution. The solution was concentrated to dryness, producing a lime colored residue, which was dissolved into a minimum of hot methanol. The solution was left open to the atmosphere, and slow evaporation provided brown rod crystals, which were isolated by vacuum filtration, yield: 0.060 g (51%). Anal. Calcd for $C_{34}H_{23}N_3O_6F_{12}$-Cu (Found): C, 47.40 (47.30); H, 2.69 (2.74); N, 4.88 (4.87). MS (FAB +): 653 (M − hfac, 100), 446 (M − 2hfac, 30), 383 (**1**, 55%). FT-IR (film, KBr): 1653 (m), 1589(w), 1548 (m), 1508 (s), 1471 (s), 1442 (m), 1348 (w), 1254 (s), 1200 (s), 1144 (s), 1082 (m), 1031 (w), 833 (w), 791 (m), 665 (m), 586 cm^{-1} (w). UV−vis (CH_2Cl_2), λ_{max} (ε): 394 nm (1.6 × 10^4 cm^{-1} M^{-1}).

Results and Discussion

Ligand Synthesis, Coordination Chemistry, and Structural Studies. In an effort to explore the basic coordination chemistry of triarylamminium radical cations, we have designed ligand **1**, a simple 2,2′-bipyridine derivative featuring a *N*,*N*′-(4,4′-dimethoxydiphenyl)amine substituent attached at the 5 position of the bipyridine framework. Ligand **1** is easily prepared from 5-bromo-2,2′-bipyridine via palladium-catalyzed Buchwald−Hartwig cross-coupling in toluene solution and has been fully characterized (Scheme 1). A series of neutral coordination complexes containing **1** were prepared by combination of M(hfac)$_2\cdot x$H$_2$O salts [M = Mn (**2**), Ni (**3**), Cu (**4**)] with **1** in a hexanes/CH_2Cl_2 solution (Scheme 1). All of the complexes are analytically pure microcrystals and feature very similar FT-IR absorption spectra (Figures S4, S5, and S6 in the Supporting Information). Slow evaporation of methanol solutions containing **4** produced single crystals suitable for X-ray diffraction studies. An ORTEP diagram of the molecular structure of **4** is shown in Figure 3. This structure features the anticipated Jahn−Teller distorted, *cis* pseudo-octahedral coordination geometry about Cu^{2+}, with **1** binding as a bidentate ligand through the bipyridine ring nitrogen atoms. Coordinate bond lengths and angles are listed in the Figure 2 caption and are in the anticipated range, with two longer bonds and four shorter. Other bond distances and angles within the hfac ancillary ligands are unremarkable and are provided in the Supporting Information. One structural feature of note is the near planarity of the neutral three-coordinate nitrogen atom (N3), featuring a bond angle sum of 359.8°. The bond to the bipyridine substituent, which is less than 1.4 Å, is the shortest of the three C−N bonds to N3. These features suggest delocalization with the 2,2′-bipyridine ring, which bodes well for electronic communication between the radical cation and the coordinated metal ion in the one-electron oxidized complex. Solutions of the radical cation complexes of **2**−**4** can be generated by one electron oxidation of the neutral precursors with $NOPF_6$ as an oxidant. The stability of these radical cation solutions is best described as persistent under a N_2 atmosphere, and the solutions gradually decompose over the course of an hour, as indicated by UV−visible spectroscopy. The stability of these solutions in air is shorter, with decomposition noted over the course of minutes.

Electronic Properties. The electronic properties of **1**−**4** have been investigated using a combination of UV−visible spectroscopy and cyclic voltammetry (CV). The UV−visible spectra of **1**−**4** are shown in Figure 4. The spectrum of **1** is similar to other reported triarylamines featuring a long wavelength $n\rightarrow\pi^*$ absorption at 350 nm along with other higher energy transitions.[23] The spectra of complexes **2**−**4** are similar to one another with the long

(23) (a) Amthor, S.; Noller, B.; Lambert, C. *Chem. Phys.* **2005**, *316*, 141–152. (b) Bushby, R. J.; Taylor, N.; Williams, R. A. *J. Mater. Chem.* **2007**, *17*, 955–964. (c) Bushby, R. J.; Kilner, C. A.; Taylor, N.; Vale, M. E. *Tetrahedron* **2007**, *63*, 11458–11466.

Scheme 1. Preparation of **1**−**4**[a]

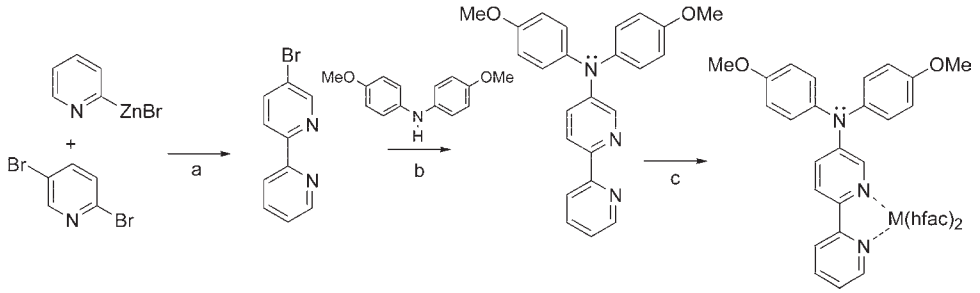

[a] Reagents and conditions: (a) 5 mol % $Pd(PPh_3)_4$, RT, 36 h. (b) 5.5 mol % $Pd(OAc)_2$, BINAP, Cs_2CO_3, toluene, 95 °C, 36 h. (c) $M(hfac)_2 \cdot xH_2O$ (M = Mn, **2**; Ni, **3**; Cu, **4**), hexanes/CH_2Cl_2, RT.

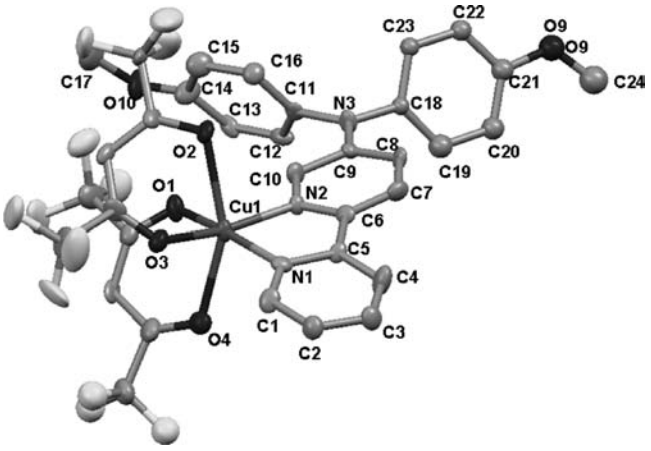

Figure 3. ORTEP diagram of the molecular structure of **4**. H atoms are omitted for clarity. One of the two crystallographically independent molecules per unit cell is shown. Selected bond distances (Å) and angles (deg): Cu(1)−O(2), 2.381(7); Cu(1)−O(1), 1.988(6); Cu(1)−O(3), 1.978(6); Cu(1)−O(4), 2.294(7); Cu(1)−N(1), 2.008(7); Cu(1)−(N2), 2.007(7); O(1)−Cu(1)−N(1), 167.3(3); O(3)−Cu(1)−N(2), 164.7(3); O(2)−Cu(1)−O(4), 155.8(2); O(1)−Cu(1)−N(2), 92.3(3); O(3)−Cu(1)−N(1), 92.8(3); O(1)−Cu(1)−O(3), 96.1(3); N(1)−Cu(1)−N(2), 81.3(3).

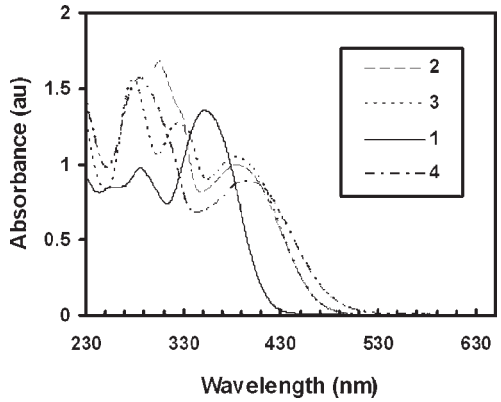

Figure 4. Room temperature UV−vis spectra of **1**−**4** in CH_2Cl_2.

wavelength band observed in **1** in all cases bathochromically shifted by approximately 30 nm.

The electrochemical properties of **1**−**4** were probed with CV. The voltammograms are featured in Figure 5, and important anodic data for all compounds are summarized in Table 2. All potentials quoted are referenced to the ferrocene/ferrocenium couple. The anodic scan of **1** features two quasi-reversible waves at +0.5 and +1.0 V, respectively. Increasing the scan rate from the original rate of 100 mV/s did not improve the reversibility of either anodic wave, which is attributed to formation of the radical cation, followed by dication formation at a higher potential. A minor feature is noted at approximately +0.7 V in the subsequent reduction cycle, which is likely attributable to a decomposition product resulting from the oxidation of **1**. The cathodic scan revealed no facile reductive processes for this ligand, as expected. These observations are in line with electrochemical data reported for other triarylamines. Anodic scans for complexes **2**−**4** are similar to one another. Of note, the formation of a radical cation (E'_{ox1}) is a reversible process in all cases, indicating that the radical cations are stabilized by coordination to the metal ion. The potential for radical cation formation is a little higher in the coordination complexes than was observed in **1**. In contrast to **2** and **3**, the anodic waves in **4** are somewhat broader, and at scan rates slower than 100 mV/s, a new irreversible feature between E'_{ox1} and E'_{ox2} is clearly noted, which disappears at faster scan rates (> 200 mV/s). We tentatively attribute this irreversible feature to an oxidation side product that decomposes prior to detection at faster scan rates. Dication formation is observed at potentials slightly greater than +1.0 V for each complex. Over cathodic potentials greater than −1.0 V, a series of irreversible processes are observed, which can be attributed to reductions involving the hfac and 2,2′-bipyridine ligands. The electrochemical properties of precursor $M(hfac)_2$ complexes have been investigated by Villamena et al. and are well understood.[24]

Spectroelectrochemical Measurements. Spectroelectrochemical spectra (Figure 6; see Scheme 2 for the electrochemical generation scheme of complexes **2**−**4**) were recorded for complexes **2**−**4** by applying a potential of approximately 1 V (versus silver wire) to solutions of the complexes in CH_2Cl_2 (containing 0.1 M $^nBu_4NPF_6$) while simultaneously recording the time-dependent absorption spectra between 250 and 1000 nm. In all cases, absorption bands assigned to the starting neutral complexes decreased in absorption intensity (down arrows) over the course of the oxidation while new bands appeared (up arrows) which are assigned to the single electron oxidized radical cation complexes. In particular, new bands at wavelengths similar to 446, 615, and 820 nm have been

(24) Villamena, F. A.; Horak, V.; Crist, D. R. *Inorg. Chim. Acta* **2003**, *342*, 125–130.

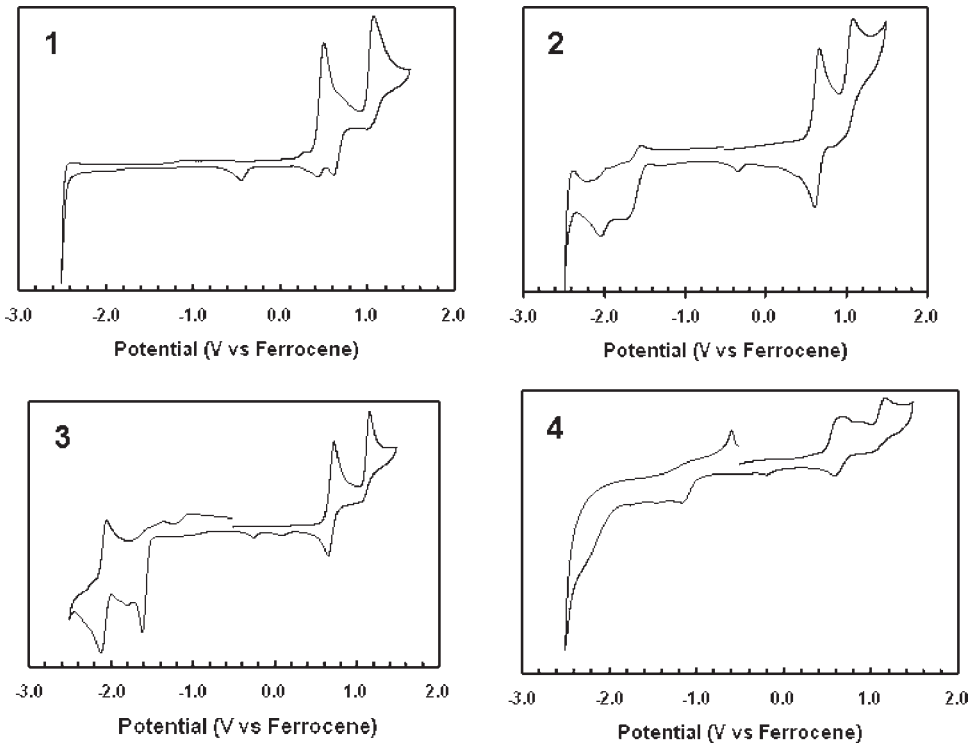

Figure 5. Cyclic voltammograms of 10^{-3} M solutions of **1**−**4** in CH_3CN containing 0.1 M Bu_4NPF_6. In all cases, the scan rate was 100 mV/s.

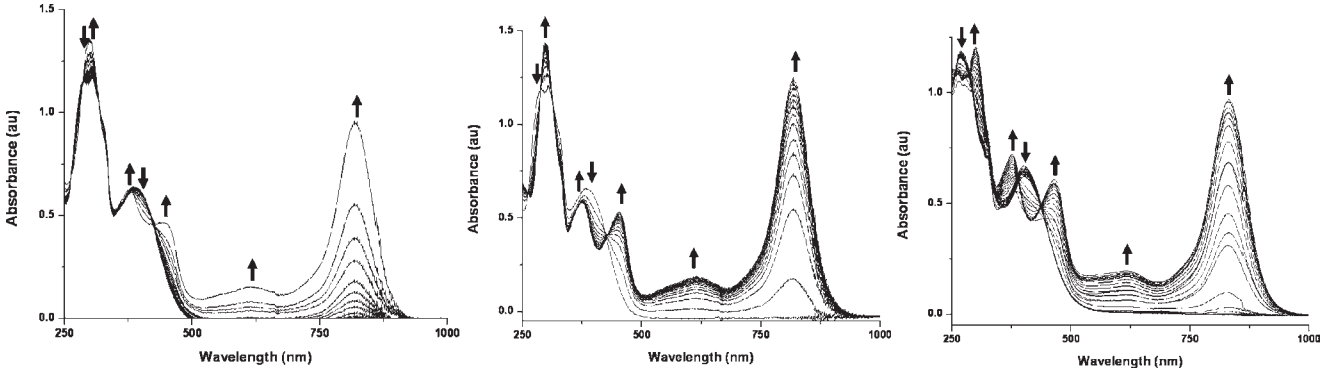

Figure 6. Spectroelectrochemistry of **2** (left), **3** (center), and **4** (right) in CH_2Cl_2 at room temperature containing 0.1 M $^nBu_4NPF_6$. A potential of +1.0 V was applied across a platinum gauze working electrode and silver wire pseudoreference electrode (platinum counter electrode). Black arrows represent the increase (up pointing) or decrease (down pointing) in absorbance over the course of the oxidation.

Table 2. Selected Electrochemical Data for Compounds **1**−**4**[a]

Compound	E'_{ox1} (V)	E'_{ox2} (V)
1	+0.5	+1.0
2	+0.6 (rev)	+1.0
3	+0.7 (rev)	+1.1
4	+0.6 (rev)	+1.1

[a] All experiments were performed in CH_3CN, containing 0.1 M $^nBu_4NPF_6$ supporting electrolyte, and all potentials are quoted versus the ferrocene/ferrocenium reference.

observed in other reported free and coordinated triarylamminum radical cations. Isosbestic points are noted in all spectra, indicating clean oxidative processess and the presence of only two species in solution over the course of the oxidation.

Variable-Temperature Magnetic Susceptibility and EPR Spectroscopy. The solid-state temperature-dependent magnetic properties of neutral complexes **2**−**4** were investigated

Scheme 2. Electrochemical Generation of Radical Cation Complexes of **1** (M = Mn, **2**; Ni, **3**; Cu, **4**)

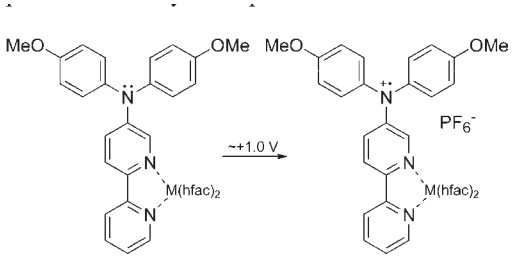

using SQUID magnetometry. As anticipated, nearly ideal Curie behavior is noted for all complexes with approximately temperature-independent magnetic moments that are typical for isolated monometallic Mn, Ni, and Cu complexes, with only very small deviations noted at the lowest temperatures (Figure 7).

The magnetic properties of the one-electron oxidized radical cations of **2** and **3** were measured in solution using the Evans method (Figure 8). For comparison, the magnetic moments for neutral complexes **2** and **3** were also measured by this technique. Data were recorded from 300 to 244 K for **2** and $\mathbf{2}^{+\bullet}$ and from 325 to 244 K for **3** and $\mathbf{3}^{+\bullet}$ (low-temperature data collection is limited to temperatures above the freezing point of acetonitrile). The data for neutral **2** are very similar to those recorded in the solid state, with a magnetic moment of 5.9 μ_B at 300 K, which is the anticipated value for a magnetically dilute Mn^{2+}

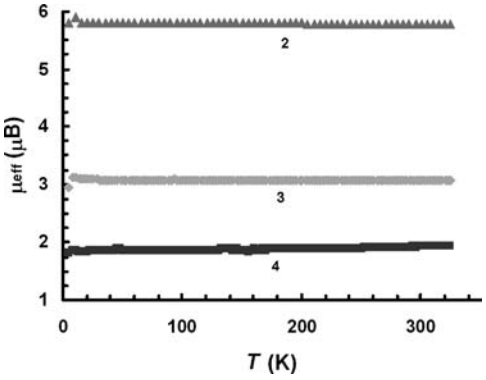

Figure 7. Temperature dependence of μ_{eff} values for **2** (▲), **3** (♦), and **4** (■) (1000 Oe field).

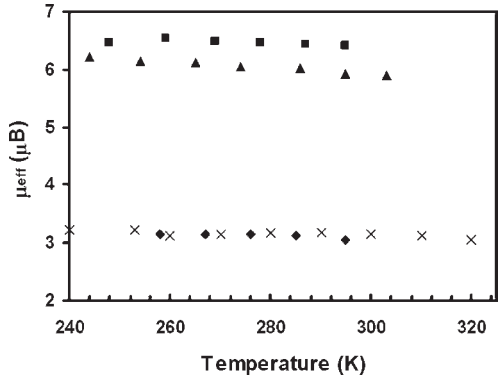

Figure 8. Temperature dependence of μ_{eff} values for **2** (▲), $\mathbf{2}^{+\bullet}\mathbf{PF_6}^-$ (■), **3** (×), and $\mathbf{3}^{+\bullet}\mathbf{PF_6}^-$ (♦) measured in solution by the Evans method.

complex. However, the magnetic moment of the singly oxidized $\mathbf{2}^{+\bullet}PF_6^-$ complex is higher, approaching 6.4 μ_B This value is also higher than the theoretical value anticipated for noninteracting $S = 5/2$ Mn^{2+} and a coordinated radical ($S = 1/2$), which is 6.16 μ_B and suggests the presence of ferromagnetic coupling between Mn^{2+} and the radical. While at low temperatures, a freshly prepared solution of $\mathbf{3}^{+\bullet}$ was placed in the spectrometer, and an identical Evans experiment was run from low to higher temperatures. The initial magnetic moment of the sample was 3.1 μ_B, which is a little lower than the anticipated value (3.3 μ_B) for noninteracting $S = 1$ Ni^{2+} and a coordinated radical ($S = 1/2$). Our data support the presence of weak Ni^{2+}−radical antiferromagnetic coupling. For comparison, Evans data were acquired for an acetonitrile solution of neutral complex **3**, and the data are very similar to those obtained from the solid-state experiment. The magnetic properties of oxidized **4** were not investigated because the cyclic voltammetry results for this complex indicated an unclean oxidation. Solution EPR spectra of **4** and $\mathbf{4}^{+\bullet}$ recorded in toluene at 298 K are included in the Supporting Information (Figure S7).

Spin Density Calculations. Density functional calculations at the B3LYP/TZVP level were used to calculate the structures and spin density distributions for the ground state singly oxidized radical cation complexes. The ground state spin density distributions within the radical cation complexes of **2**−**4** are shown in Figure 9. For complex $\mathbf{2}^{+\bullet}$, a substantial positive π spin density is noted at the amminium nitrogen atom, and the π spin distribution around each atom of the adjacent bipyridine ring alternates negative then positive. The 2,2′-bipyridine coordinating nitrogen atom features a significant amount of negative π spin density, which results in positive d_π spin density at Mn^{2+}, which produces an overall ferromagnetic interaction between the radical and Mn^{2+} ion. On the other hand, complexes $\mathbf{3}^{+\bullet}$, and $\mathbf{4}^{+\bullet}$ feature metal ions with d_σ spin density of the same sign as the π spin density at the coordinate nitrogen atom, and the net interaction with the radical in each case is antiferromagnetic. These results are similar to the pioneering studies of Iwamura et al., which elegantly demonstrated the spin polarization mechanism behind the magnetic coupling in a series of $M(hfac)_2$ complexes featuring differentially

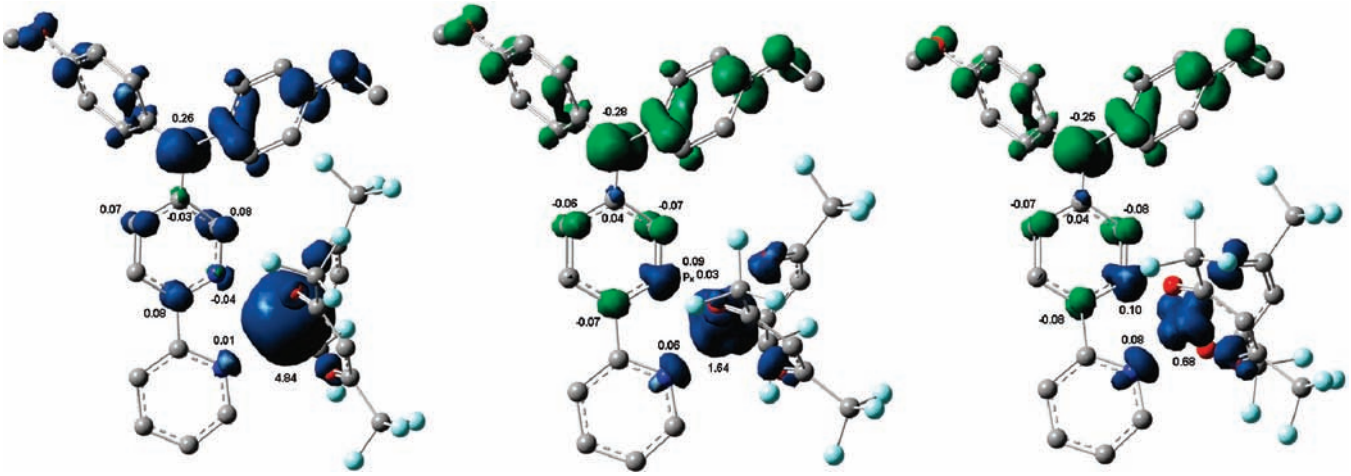

Figure 9. Calculated spin density distributions for $\mathbf{2}^{+\bullet}$ (left), $\mathbf{3}^{+\bullet}$ (center), and $\mathbf{4}^{+\bullet}$ (right). NPA-derived atomic spin density is shown for most important contributors. H atoms are not shown for clarity.

substituted pyridine or 2,2′-bipyridine-containing nitroxide radicals.[25,26]

Conclusions

The results presented herein represent our initial efforts toward exploring the coordination chemistry of triarylamminium radical cations. We are actively designing ligands in which the triarylamminium spin density is polarized toward the metal center in an effort to engineer stronger metal−radical exchange coupling. We have observed ferromagnetic metal−radical coupling in oxidized complex **2**, and we are currently trying to exploit and enhance this interaction in polymetallic complexes. Using this approach, we can engineer ferromagnetic interactions with transition metals containing d_σ magnetic orbitals by simple synthetic adjustment of the triarylamminium radical cation on the 2,2′-bipyridine ring. For example, similar complexes to **3** and **4**, but containing instead a 4- or 6-substituted 2,2′-bipyridine triarylamminium ligand, should result in ferromagnetic metal−radical interactions (M = Ni or Cu). We are also investigating the feasibility of enhancing the stability of the triarylamminium cation complexes, through steric protection of the spin density rich sites in an effort to isolate crystalline metal−radical complexes to obtain solid-state structural and magnetic susceptibility data. These efforts are underway and will be published in due course.

Acknowledgment. The authors acknowledge NSERC (Discovery & RTI) and CFI (Leaders Opportunity Fund) for financial support. We thank Razvan Simionescu (Brock University) for help with the Evans method experiments.

Supporting Information Available: General spectroscopic data and crystallographic data in CIF format. This material is available free of charge via the Internet at http://pubs.acs.org.

(25) (a) Kitano, M.; Ishimaru, Y.; Inoue, K.; Koga, M.; Iwamura, H. *Inorg. Chem.* **1994**, *33*, 6012–6019. (b) Ishimaru, Y.; Kitano, M.; Kumada, H.; Koga, N.; Iwamura, H. *Inorg. Chem.* **1998**, *37*, 2273–2280. (c) Kumada, H.; Sakane, A.; Koga, N.; Iwamura *J. Chem. Soc., Dalton Trans.* **2000**, *10*, 911–914.
(26) Shimada, T.; Ishida, T.; Nogami, T. *Polyhedron* **2005**, *24*, 2593–2598.